REDOX VARIATIONS AT COLD SEEPS RECORDED BY RARE EARTH ELEMENTS IN SEEP CARBONATES

Dong Feng, Duofu Chen∗, Zhijia Lin
Key Laboratory of Marginal Sea Geology
Guangzhou Institute of Geochemistry, Chinese Academy of Sciences
Guangzhou, 510640

Graduate university of Chinese Academy of Sciences
Beijing 100049
CHINA

Jörn Peckmann, Gerhard Bohrmann
MARUM, University of Bremen
Post Box 330 440, D-28334 Bremen, GERMANY

Harry H. Roberts
Coastal Studies Institute, Louisiana State University
Baton Rouge, LA 70803, USA

ABSTRACT

Understanding the formation conditions of seep carbonate is crucial to better constrain the dynamic fluid flow and chemical fluxes associate with cold seeps on the seafloor. Rare earth element (REE) in seep carbonates collected from modern cold seeps of Gulf of Mexico, Black Sea, Congo Fan, ancient seeps of Beauvoisin (Oxfordian, J_3, Southeastern France) and Marmorito (Miocene, Northern Italy) were studied. Our focus has been on 5% HNO_3-treated solution (authigenic carbonate minerals) of carbonates. Several crystalline forms of carbonate minerals have been selected for analysis. Total REE (∑REE) contents in seep carbonates varies widely, from 0.068 to 43.655 ppm, but the common trend is that the ∑REE in microcrystalline phases is highest and lowest of in sparite, suggesting that the ∑REE of seep carbonates may be a function of diagenesis. The shale-normalized REE patterns of the seep carbonates show varied Ce anomalies across several seep sites and even within one site, suggesting that the formation condition of seep carbonate is variable and complex. Overall, our results show that apart from anoxic, oxic formation condition is also common at hydrocarbon seep environments.

Keywords: cold seep, rare earth element, redox variation, seep carbonate

INTRODUCTION
Seep carbonate precipitation is a widely observed phenomenon in the modern and ancient marine seep environments of the world *[1-3]*. Carbonate precipitation at cold seep sites is a result of microbial oxidation of methane, as well as higher

---

∗ Corresponding author: Phone: +86 20 8529 0286 Fax +86 20 8529 0130 E-mail: cdf@gig.ac.cn

molecular weight hydrocarbons, through the combined metabolism of methane oxidizing archaea (MOA) and sulfate reducing bacteria (SRB) [4-6].

Seafloor observations of cold seep sites show that the chemical and physical characters of cold seep sites are complex and variable [7] and [8]. However, it is difficult to trace this dynamic characterization, especially the variation of redox condition induced by bacterial processes at modern and ancient cold seeps. The Ce anomaly of authigenic sediment deposited at the seafloor is an effective indicator of the sedimentary redox variation [9-11]. Here we report rare earth element (REE) in 5% HNO_3-treated solution (authigenic carbonate mineral) of seep carbonates collected from modern seeps of Congo Fan, Black Sea, Gulf of Mexico, ancient seep from Beauvoisin (Oxfordian, J_3, Southeastern France) and Marmorito (Miocene, Northern Italy). Our aim has been to trace the variation in redox conditions during seep carbonate precipitation.

MATERIALS AND METHODS

Seep carbonates analyzed in this paper were recovered from three modern seep areas: Bush Hill (540 m water depth) and Alaminos Canyon (2200 m water depth) of Gulf of Mexico, Romania shelf (120 m water depth) and Ukraine slope (190 m water depth) of Black Sea, Hydrate Hole (3113 m water depth) and Diapir Field (2417 m water depth) of Congo Fan, two ancient seeps of Beauvoisin (Oxfordian, J_3, Southeastern France) and Marmorito (Miocene, Northern Italy) (Table 1).

The 0.1 to 0.5 g sample powder was treated with 50 ml of 5% HNO_3 in a centrifuge tube for 2-3 hours to separate the carbonate mineral phase and residue phase. Then, 2500 ng of Rhodium was added as an internal standard for calculating the element concentration of dissolved carbonate mineral phase. Five milliliters of this solution was further diluted 10 times to be used for the REE analysis using Finnigan MAT ELEMENT high resolution ICP-MS. Precision of the REE analysis was checked by multiple analyses of standard samples. The average standard deviations are less than 10%, and average relative standard deviations are better than 5%. For detail of the analyses see Qi et al. [15].

In this paper, Ce/Ce* denotes $3Ce_N/(2La_N+Nd_N)$, where N refers to normalization of concentration against the standard Post Archean Australian Shale (PAAS) [9]. Ce_{anom} denotes $Log(Ce/Ce*)$, Ce_{anom} >-0.1 is positive anomaly, which means anoxic formation condition, while Ce_{anom} <-0.1 is negative anomaly, which means oxic formation condition [10].

RESULTS AND DISCUSSION
Seep carbonate of Gulf of Mexico
Bush Hill seep carbonates: The total REE content (∑REE) is 7.070~26.565 ppm for microcrystalline and 0.402~3.096 ppm for sparite. The ∑REE in microcrystalline is higher than that of in sparite for the same sample (Table 2). The shale-normalized REE patterns show varied Ce anomalies, from negative (Ce_{anom}=-0.615~-0.100) to positive (Ce_{anom}= -0.062~-0.006) (Table 2 and Figure 1) between different samples and even in one sample (BH-A).

The varied Ce anomalies between samples and even in the different carbonate phases of the same sample (microcrystalline and sparite, e.g. BH-A) strongly indicated the spatial and temporal change of the precipitation conditions of seep carbonate [12]. We suggest that the rate of fluid flow at Bush Hill seep site may be the primary factor that controls redox variations in seep environment. During conditions of relatively slow seepage, the carbonate precipitation occurs deep below the water/sediment interface, where the formation conditions are anoxic, yielding carbonates with positive Ce anomalies. On the other hand, higher seepage rates cause methane to be transported into the shallow sediments or even in the water, where conditions are relatively oxic, and the carbonates show negative Ce anomalies.

Alaminos Canyon seep carbonates: The ∑REE is 12.725 ppm for microcrystalline and 2.227 ppm for sparite. Similar to seep carbonate at Bush Hill, the ∑REE in microcrystalline is higher than that of in sparite (Table 2). The shale-normalized REE patterns show distinct negative Ce anomalies (Ce_{anom}=-0.349~-0.294) (Table 2 and Figure 1), indicating that the seep carbonates formed under oxic conditions, which may be related to the dynamic characterization of the cold seeps [13].

Seep carbonate of Black Sea
Romania shelf seep carbonates: The ∑REE of seep carbonates is very low, 2.026 ppm for microcrystalline, 0.896 ppm for microspar and 0.552 ppm for sparite (Table 2). The shale-normalized REE patterns show negative Ce anomalies (Ce_{anom}=-0.218~-0.100) (Table 2 and

Figure 1), indicates that the Romania shelf seep carbonates formed under oxic conditions.

Ukraine slope seep carbonates: Similar to the Romania shelf seep carbonates, the $\sum$REE of Ukraine slope seep carbonates is very low, 2.817 ppm for microcrystalline, 0.695 ppm for microspar and 0.068 ppm for sparite (Table 2). But, unlike to the Romania shelf seep carbonates, the shale-normalized REE patterns of Ukraine slope seep carbonates show positive Ce anomalies (Ce_{anom}=-0.053~0.014 (Table 2 and Figure 1), indicates that the Ukraine slope seep carbonates formed under anoxic conditions.

It is suggested from the REE patterns that Romania shelf and Ukraine slope seep carbonates formed under oxic and anoxic conditions, respectively. Which is consistent with the obvious oxygen value (11 μmol/L) in the bottom water of Romania shelf, and no oxygen was detected in bottom water of Ukraine slope *[3]*. Thus, there should be an oxic–anoxic interface between the depth from Romania shelf to Ukraine slope during the formation of those seep carbonates.

Seep carbonate of Congo Fan

Hydrate Hole seep carbonate: The $\sum$REE is 23.173~42.539 ppm for microcrystalline, 23.461~30.986 ppm for microspar and 1.59 ppm for sparite (Table 2). The shale-normalized REE patterns show distinct positive Ce anomalies (Ce_{anom}=0.188~0.266) (Table 2 and Figure 1), indicates that the Hydrate Hole seep carbonates formed under anoxic conditions.

Diapir Field seep carbonate: The $\sum$REE is 41.636 ppm for microcrystalline (Table 2). Similar to Hydrate Hole, the shale-normalized REE pattern shows positive Ce anomalies (Ce_{anom}=0.105) (Table 2 and Figure 1), indicates that the Diapir Field seep carbonates also formed under anoxic conditions.

It is obvious that Hydrate Hole and Diapir Field seep carbonates formed under anoxic conditions. This is confirmed by the depleted $\delta^{13}C_{PDB}$ values from -60.2 to -48.2 of those seep carbonates, which clearly indicates that the carbon is derived from a methane source and carbonate precipitation was due to anaerobic methane oxidation (Table 1), further evidence is also from biomarker analyses *[14]*.

Seep carbonate of Marmorito

The $\sum$REE of seep carbonates is 5.220~43.655 ppm for microcrystalline, 3.220~7.177 ppm for microspar, 0.992~1.031 ppm for sparite, and 2.416 ppm for blocky cement. The shale-normalized

REE patterns show varied Ce anomalies, from negative (Ce_{anom}=-0.435~-0.134) to positive (Ce_{anom}=-0.099~-0.029) Ce anomalies (Table 2 and Figure 1) between different samples. The varied Ce anomalies between samples indicates that the spatial or/and temporal change of the precipitation conditions of Marmorito seep carbonates. Remarkably, apart from lipid biomarkers of MOA and SRB, biomarkers of aerobic methanotrophic bacteria have been found in this rock *[2]* and *[16]*.

Seep carbonate of Beauvoisin

The $\sum$REE is 11.430~21.005 ppm for microcrystalline, 16.847~24.773 ppm dolomite, and 3.32 ppm for sparite (Table 2). The shale-normalized REE patterns show distinct positive Ce anomalies (Ce_{anom}=-0.066~0.037) (Table 2 and Figure 1), indicates that the Beauvoisin seep carbonates formed under anoxic conditions.

SUMMARY

The $\sum$REE of carbonates from modern seeps of Gulf of Mexico, Black Sea, Congo Fan, ancient seeps from Beauvoisin (Oxfordian, J_3, Southeastern France) and Marmorito (Miocene, Northern Italy) has a wide range, from 0.068 to 43.655 ppm, but usually less than 10 ppm. The common trend is that the $\sum$REE in microcrystalline phases is higher than in sparite, suggesting that the REE content of seep carbonate may be a function of diagenesis. The shale-normalized REE patterns of the seep carbonates show varied Ce anomalies, indicating the different formation conditions. Congo Fan and Beauvoisin seep carbonates formed under anoxic condition, Black Sea seep carbonates formed under oxic (120 m water depth) and anoxic (190 m water depth) condition, while Gulf of Mexico and Marmorito seep carbonates formed under both anoxic and oxic condition, suggesting that the formation condition of the seep carbonate is variable and complex.

Overall, our results show that apart from anoxic, oxic formation condition is also common in hydrocarbon seep environments. The carbonate precipitation under oxic condition may be related to a decrease of seepage rates. When the seep rate decreases, the interface of oxic and anoxic conditions migrates downwards, thus the HCO_3^- in former anoxic zone will continue to precipitate carbonate. Furthermore, the intermittent variation of the seepage rate may also result in the carbonate precipitation under aerobic conditions. The HCO_3^- produced in deep anaerobic zone could be brought

Location	Sampling information	Age	Carbonate microfabrics	$\delta^{13}C_{PDB}$ ‰	References
Gulf of Mexico	*Bush Hill (GC185, 27°46'N; 91°30'W):* Johnson-Sea-Link I Submersible dive 2904 (1997), 4061 (1998) and 4063 (1998), 540 m water depth	Modern (0.8~10 ka)	Microcrystalline aragonite, clotted micrite, banded/botryoidal aragonite cement	-29.4~-15.1	*[12]*
	Alaminos Canyon 645 (26°21'N/94°31'W): *DSV Alvin* Submersible dive 2209 (1990), 2200 m water depth	Modern (10.6~11.6 ka)	Microcrystalline aragonite, clotted micrite, banded/botryoidal aragonite cement	-31.3~-23.4	*[13]*
Black Sea	*Romanian shelf:* R/V *Poseidon* cruise (1994), 120 m water depth	Modern	Microcrystalline high-Mg-calcite or aragonite, and aragonite cement	-37.3~-28.9	*[3]*
	Ukraine slope: R/V Professor cruise (1993, 1994), 190 m water depth	Modern	microcrystalline high-Mg-calcite or aragonite, and aragonite cement	-41.0~-14.8	*[3]*
Congo Fan	*Hydrate Hole (04°48'56"S/09°54'50"E):* R/V Meteor M56-B Cruise (2002), 3113 m water depth	Modern	Microcrystalline aragonite and high-Mg calcite, pure aragonite	-60.2~-48.2	*[14]*
	Diapir field (06°11'04"S/10°25'53"E): R/V Meteor M56-B Cruise (2002), 2417 m water depth	Modern	Microcrystalline aragonite and high-Mg calcite		
Northern Italy	*Marmorito:* Cold seep deposits occur near the village of Marmorito in the Monferrato hills, east of Torino in northern Italy	Miocene	Microcrystalline dolomite, calcitic veins, botryoidal aragonite, in situ brecciation	-40.2~-17.3	*[2]*
Southeastern France	*Beauvoisin:* Located in southeastern France near Buisles-Baronnies	Oxfordian (J_3)	Microcrystalline high-Mg-calcite and botryoidal aragonite	-26.5~+15.1	*[2]*

Table 1. Background information of the studied samples.

Number[++]	Type[+]	La	Ce	Pr	Nd	Sm	Eu	Gd	Tb	Dy	Ho	Er	Tm	Yb	Lu	∑REE	Ce/Ce*	Ce$_{anom}$
BH-A-1	mi	2.935	5.406	0.695	2.748	0.627	0.135	0.530	0.087	0.471	0.090	0.253	0.037	0.209	0.031	14.253	0.868	-0.062
BH-A-2	sp	0.521	0.863	0.122	0.465	0.097	0.023	0.092	0.013	0.079	0.015	0.042	0.005	0.035	0.005	2.377	0.794	-0.100
BH-B-1	mi	3.726	7.309	0.922	3.585	0.748	0.164	0.579	0.093	0.513	0.091	0.249	0.035	0.209	0.030	18.254	0.916	-0.038
BH-C-1	mi	6.086	5.734	1.275	5.213	0.859	0.164	0.541	0.086	0.409	0.075	0.204	0.025	0.159	0.022	20.852	0.457	-0.340
BH-C-2	sp	1.004	0.782	0.190	0.731	0.116	0.023	0.096	0.012	0.062	0.011	0.034	0.004	0.026	0.004	3.096	0.397	-0.401
BH-D-1	mi	4.928	5.421	1.033	4.170	0.711	0.149	0.508	0.075	0.369	0.070	0.190	0.024	0.170	0.021	17.840	0.536	-0.271
BH-D-2	sp	0.113	0.055	0.024	0.092	0.021	0.005	0.023	0.003	0.025	0.005	0.016	0.002	0.014	0.003	0.402	0.242	-0.615
BH-F-1	mi	1.279	2.793	0.374	1.400	0.312	0.066	0.282	0.040	0.241	0.042	0.122	0.014	0.092	0.013	7.070	0.973	-0.294
BH-F-2	sp	0.173	0.328	0.044	0.164	0.035	0.008	0.036	0.005	0.026	0.005	0.015	0.002	0.011	0.002	0.853	0.889	-0.349
BH-G-1	mi	5.307	10.59	1.326	5.154	1.078	0.239	0.945	0.143	0.798	0.147	0.386	0.059	0.340	0.050	26.565	0.929	-0.650
BH-H-1	mi	2.298	5.123	0.668	2.553	0.567	0.080	0.511	0.077	0.444	0.079	0.220	0.030	0.191	0.028	12.870	0.987	-0.012
AC-1	mi	3.410	3.627	0.709	3.068	0.566	0.123	0.380	0.071	0.338	0.058	0.184	0.025	0.146	0.019	12.725	0.508	-0.051
AC-2	sp	0.595	0.545	0.118	0.499	0.104	0.023	0.101	0.016	0.097	0.018	0.054	0.007	0.044	0.007	2.227	0.448	-0.081
BS-RO-1	mi	0.355	0.595	0.099	0.412	0.110	0.028	0.114	0.018	0.113	0.023	0.072	0.009	0.067	0.010	2.026	0.730	-0.032
BS-RO-2	ms	0.198	0.247	0.040	0.170	0.034	0.009	0.044	0.007	0.051	0.011	0.038	0.005	0.036	0.006	0.896	0.606	0.332
BS-RO-3	sp	0.109	0.172	0.019	0.083	0.017	0.004	0.027	0.004	0.034	0.009	0.032	0.004	0.031	0.005	0.552	0.794	-0.006
BS-UKR-1	mi	0.487	1.072	0.123	0.517	0.128	0.032	0.136	0.021	0.133	0.024	0.070	0.009	0.057	0.008	2.817	0.992	-0.137
BS-UKR-2	ms	0.130	0.271	0.024	0.103	0.023	0.006	0.031	0.005	0.033	0.008	0.026	0.004	0.027	0.004	0.695	1.033	-0.218
BS-UKR-3	sp	0.016	0.025	0.002	0.009	0.002	0.000	0.003	0.000	0.003	0.001	0.003	0.001	0.003	0.000	0.068	0.885	-0.100
CF-HH-2a-1	sp	0.194	0.885	0.073	0.269	0.055	0.030	0.053	0.007	0.035	0.006	0.017	0.002	0.017	0.002	1.586	1.844	0.266
CF-HH-2a-2	ms	3.230	0.885	1.033	4.037	0.839	0.291	0.701	0.109	0.576	0.107	0.279	0.040	0.244	0.033	23.461	1.562	0.194
CF-HH-2a-3	mi	4.497	11.94	1.472	5.951	1.205	0.402	1.079	0.166	0.931	0.169	0.436	0.061	0.366	0.051	33.599	1.542	0.188
CF-HH-2b-1	sp	2.137	16.81	0.612	2.300	0.472	0.103	0.373	0.065	0.350	0.066	0.199	0.030	0.187	0.027	14.360	1.560	0.193
CF-HH-2b-2	ms	4.461	7.439	1.336	4.939	1.041	0.234	0.884	0.137	0.734	0.141	0.381	0.054	0.336	0.047	30.986	1.616	0.208
CF-HH-2b-3	mi	6.126	16.26	1.791	7.096	1.468	0.318	1.244	0.197	1.055	0.205	0.539	0.080	0.430	0.065	42.539	1.559	0.193
CF-DF-2c	mi	6.704	21.93	1.860	7.598	1.537	0.346	1.358	0.209	1.103	0.228	0.609	0.081	0.510	0.078	41.636	1.272	0.105
CF-HH-2d	mi	3.172	19.42	1.040	3.856	0.773	0.329	0.647	0.104	0.610	0.091	0.247	0.034	0.192	0.026	23.173	1.623	0.210

Mar E-1	mi	1.329	2.680	0.329	1.349	0.309	0.067	0.236	0.048	0.249	0.048	0.141	0.020	0.122	0.017	6.945	0.923	-0.035
Mar E-2	ms	1.383	2.818	0.339	1.396	0.302	0.070	0.215	0.052	0.262	0.044	0.137	0.021	0.119	0.017	7.177	0.935	-0.029
Mar E-3	sp	0.258	0.385	0.043	0.154	0.031	0.008	0.041	0.006	0.042	0.008	0.026	0.003	0.022	0.004	1.031	0.804	-0.095
Mar E-4	bc	0.613	0.907	0.099	0.369	0.073	0.019	0.090	0.013	0.090	0.019	0.057	0.007	0.052	0.008	2.416	0.796	-0.099
Mar ES1-1	mi	11.48	12.08	2.259	9.324	1.990	0.451	1.915	0.316	1.676	0.349	0.902	0.121	0.688	0.103	43.655	0.520	-0.284
Mar ES1-2	ms	3.378	2.182	0.418	1.595	0.292	0.075	0.346	0.064	0.357	0.077	0.234	0.033	0.182	0.028	9.262	0.367	-0.435
Mar G-1	mi	1.515	1.599	0.247	1.046	0.209	0.044	0.148	0.031	0.155	0.031	0.092	0.013	0.081	0.011	5.220	0.547	-0.262
Mar G-2	ms	1.010	0.751	0.177	0.674	0.136	0.031	0.138	0.019	0.121	0.024	0.069	0.008	0.053	0.008	3.220	0.389	-0.410
Mar G-3	sp	0.215	0.327	0.048	0.187	0.041	0.010	0.041	0.007	0.048	0.009	0.027	0.003	0.024	0.003	0.992	0.734	-0.134
Mar G-4	sp	0.076	0.111	0.016	0.060	0.013	0.002	0.015	0.002	0.013	0.003	0.009	0.001	0.007	0.001	0.329	0.726	-0.139
Bea A2-1	mi	4.276	8.000	0.997	4.317	0.864	0.186	0.767	0.131	0.690	0.130	0.324	0.044	0.247	0.035	21.005	0.859	-0.066
Bea 97-1	sp	0.544	1.373	0.161	0.646	0.148	0.000	0.137	0.021	0.135	0.023	0.069	0.007	0.049	0.007	3.321	1.088	0.037
Bea 97-2	mi	2.269	4.494	0.528	2.237	0.453	0.117	0.421	0.071	0.382	0.071	0.223	0.023	0.125	0.017	11.430	0.917	-0.038
Bea 97-3-1	do	3.930	9.966	1.291	5.038	1.086	0.223	1.058	0.174	0.940	0.174	0.434	0.056	0.358	0.045	24.773	1.060	0.025
Bea 97-3-2	do	2.498	6.570	0.920	3.641	0.762	0.130	0.779	0.113	0.687	0.122	0.334	0.038	0.222	0.030	16.847	1.040	0.017

[++]BH=Bush Hill of Gulf of Mexico; AC=Alaminos Canyon of Gulf of Mexico; BS-RO=Romania shelf of Black Sea; BS-UKR=Ukraine slope of Black Sea; CF-HH=Hydrate Hole of Congo Fan; CF-DF=Diapir Field of Congo Fan; Mar=Marmorito of Northern Italy; Bea=Beauvoisin of Southeastern France.

[+]mi=microcrtstalline, ms=microspar, sp=sparite, bc=blocky cement, do=dolomite.

Table 2. Rare earth elements (REE) content (ppm) of 5% HNO_3-soluble parts of seep carbonates samples.
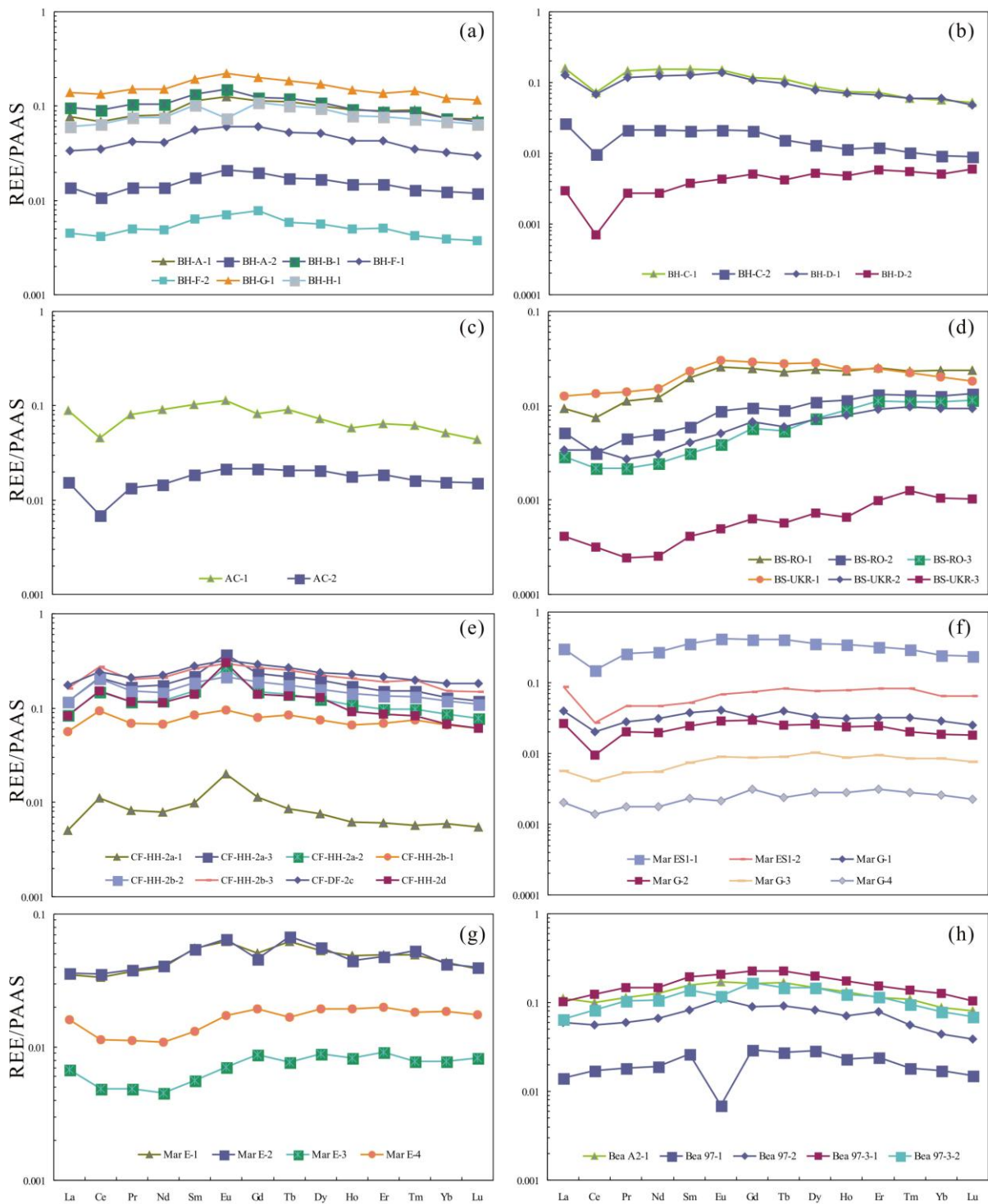
(a) and (b): Bush Hill seep carbonates show varied Ce anomalies, from positive to negative Ce anomalies between different samples and even in the same sample (BH-A); (c): Alaminos Canyon seep carbonates show negative Ce anomalies; (d): Black Sea seep carbonates show negative (BS-RO) and positive (BS-UKR) Ce anomalies; (e): Congo Fan seep carbonates show distinct positive Ce anomalies; (f) and (g): Marmorito seep carbonates show negative (Mar-ES1 and Mar G) and positive (Mar E) Ce anomalies; (h): Beauvoisin seep carbonates show positive Ce anomalies.

Figure 1 Shale-normalized REE patterns of modern and ancient cold seep carbonates

up to the subsurface oxic zone to precipitate carbonate during the stage of fast seepage. Additional geochemical data, e.g. high resolution Sr and Ba profiles of fast and slow fluid flow precipitation, is needed to further investigate the current model.

ACKNOWLEDGEMENT

REFERENCES

[1] Campbell K A. *Hydrocarbon seep and hydrothermal vent paleoenvironments and paleontology: Past developments and future research directions*. Palaeogeography, Palaeoclimatology, Palaeoecology, 2006, 232: 362-407.

[2] Peckmann J, Thiel V, Michaelis W, et al. *Cold seep deposits of Beauvoisin (Oxfordian; southeastern France) and Marmorito (Miocene; northern Italy): microbially induced authigenic carbonates*. International Journal of Earth Sciences, 1999, 88: 60-75.

[3] Peckmann J, Reimer A, Luth U, et al. *Methane-derived carbonates and authigenic pyrite from the northwestern Black Sea*. Marine Geology, 2001, 177: 129-150.

[4] Hinrichs K U, Hayes J M, Sylva S P, et al. *Methane-consuming archaebacteria in marine sediments*. Nature, 1999, 398: 802-805.

[5] Boetius A, Ravenschlag K, Schubert C J, et al. *A marine microbial consortium apparently mediating anaerobic oxidation of methane*. Nature, 2000, 407: 623-626.

[6] Valentine D L, Reeburgh W S. *New perspectives on anaerobic methane oxidation*. Environmental Microbiology, 2000, 2: 477-484.

[7] Tryon M D, Brown K M. *Fluid and chemical cycling at Bush Hill: Implications for gas and hydrate-rich environments*. Geochemistry Geophysics Geosystems, 2004, 5: 12004.

[8] Leifer I, MacDonald I. *Dynamics of the gas flux from shallow gas hydrate deposits: interaction between oily hydrate bubbles and the oceanic environment*. Earth and Planetary Science Letters, 2003, 210: 411-424.

[9] McLennan S M. *Rare earth elements in sedimentary rocks: influence of provenance and sedimentary processes*. In: Lipin B R, McKay G A, editor. Geochemistry and Mineralogy of Rare Earth Element*s*, Reviews in Mineralogy, 1989. p. 169-200.

[10] Wright J, Schrader H, Holser W T. *Paleoredox variations in ancient oceans recorded by rare earth elements in fossil apatite*. Geochimica et Cosmochimica Acta, 1987, 51: 631-644.

[11] Chen D F, Dong W Q, Qi L, et al. *Possible REE constraints on the depositional and diagenetic environment of Doushatuo Formation phosphorites containing the earliest metazoan fauna*. Chemical Geology, 2003, 201: 103-118.

[12] Feng D, Chen D F, Roberts H H. *Petrographic and geochemical characterization of seep carbonate from Bush Hill (GC185) gas vent and hydrate site of the Gulf of Mexico*. Marine and Petroleum Geology, submitted.

[13] Feng D, Chen D F, Qi L, et al. *Petrographic and geochemical characterization of seep carbonate from Alaminos Canyon, Gulf of Mexico*. Chinese Science Bulletin, 2008, in press.

[14] Blinova V, Elvert M, Teichert B M A, et al. *Fluid venting and methane-related authigenic carbonates in the pockmark area at the Northwest African margin off Congo*. Geophysical Research Abstracts, 2004, 6, 04733.

[15] Qi L, Zhou M, Malpas J, et al. *Determination of rare earth elements and Y in ultramafic rocks by ICP-MS after preconcentration using $Fe(OH)_3$ and $Mg(OH)_2$ coprecipitation*. Geostandards and Geoanalytical Research, 2005, 29: 131-141.

[16] Birgel D, Elvert M, Han X, et al. ^{13}C-depleted biphytanic diacids as tracers of past anaerobic oxidation of methane. Organic Geochemistry, 2008, 39: 152-156.